Monthly Notices of the ROYAL ASTRONOMICAL SOCIETY

MNRAS **509,** 5340–5356 (2022) https://doi.org/10.1093/mnras/stab2943
Advance Access publication 2021 October 14

Two c's in a pod: cosmology-independent measurement of the Type Ia supernova colour–luminosity relation with a sibling pair

Rahul Biswas [1]★ Ariel Goobar [1]★ Suhail Dhawan [1,2] Steve Schulze [1] Joel Johansson,[1] Eric C. Bellm,[3] Richard Dekany,[4] Andrew J. Drake,[5] Dmitry A. Duev [5] Christoffer Fremling,[5] Matthew Graham [5] Young-Lo Kim,[6] Erik C. Kool [7] Shrinivas R. Kulkarni,[5] Ashish A. Mahabal [5,8] Daniel Perley [9] Mickael Rigault,[6] Ben Rusholme [10] Jesper Sollerman,[7] David L. Shupe,[10] Matthew Smith[6] and Richard S. Walters[4]

[1]*Oskar Klein Centre, Department of Physics, Stockholm University, SE-106 91 Stockholm, Sweden*
[2]*Kavli Institute for Cosmology, University of Cambridge, Madingley Road, Cambridge CB3 0HA, UK*
[3]*DIRAC Institute, Department of Astronomy, University of Washington, 3910 15th Avenue NE, Seattle, WA 98195, USA*
[4]*Caltech Optical Observatories, California Institute of Technology, Pasadena, CA 91125, USA*
[5]*Division of Physics, Mathematics, and Astronomy, California Institute of Technology, Pasadena, CA 91125, USA*
[6]*Univ Lyon, Univ Claude Bernard Lyon 1, CNRS, IP2I Lyon/IN2P3, IMR 5822, F-69622 Villeurbanne, France*
[7]*Department of Astronomy, Oskar Klein Centre, Stockholm University, Albanova, SE-10691 Stockholm, Sweden*
[8]*Center for Data Driven Discovery, California Institute of Technology, Pasadena, CA 91125, USA*
[9]*Astrophysics Research Institute, Liverpool John Moores University, IC2, Liverpool Science Park, 146 Brownlow Hill, Liverpool L3 5RF, UK*
[10]*IPAC, California Institute of Technology, 1200 E. California Blvd, Pasadena, CA 91125, USA*

Accepted 2021 October 2. Received 2021 October 1; in original form 2021 June 29

ABSTRACT

Using Zwicky Transient Facility (ZTF) observations, we identify a pair of 'sibling' Type Ia supernovae (SNe Ia), i.e. hosted by the same galaxy at $z = 0.0541$. They exploded within 200 d from each other at a separation of 0.6 arcsec corresponding to a projected distance of only 0.6 kpc. Performing SALT2 light-curve fits to the *gri* ZTF photometry, we show that for these equally distant 'standardizable candles', there is a difference of 2 mag in their rest-frame B-band peaks, and the fainter supernova (SN) has a significantly red SALT2 colour $c = 0.57 \pm 0.04$, while the stretch values x_1 of the two SNe are similar, suggesting that the fainter SN is attenuated by dust in the interstellar medium of the host galaxy. We use these measurements to infer the SALT2 colour standardization parameter, $\beta = 3.5 \pm 0.3$, independent of the underlying cosmology and Malmquist bias. Assuming the colour excess is entirely due to dust, the result differs by 2σ from the average Milky Way total-to-selective extinction ratio, but is in good agreement with the colour–brightness corrections empirically derived from the most recent SN Ia Hubble–Lemaitre diagram fits. Thus we suggest that SN 'siblings', which will increasingly be discovered in the coming years, can be used to probe the validity of the colour and light-curve shape corrections using in SN Ia cosmology while avoiding important systematic effects in their inference from global multiparameter fits to inhomogeneous data sets, and also help constrain the role of interstellar dust in SN Ia cosmology.

Key words: dust, extinction – galaxies: distances and redshifts – distance scale – transients: supernovae.

1 INTRODUCTION

The discovery of the late-time accelerated expansion of the Universe using Type Ia supernovae (SNe Ia) as cosmological yardsticks (Riess et al. 1998; Perlmutter et al. 1999) had a profound impact on our understanding of the cosmic composition. The pioneering work of the Supernova Cosmology Project and the High-z Supernova Search Team was followed by many efforts to improve the use of SNe Ia in cosmology with the purpose to better understand the nature of dark energy (see Goobar & Leibundgut 2011, for a review). Essential for the standardization of SNe Ia to obtain precise distances are the corrections for the light-curve shape–brightness relation (Phillips 1993) and the colour–brightness relation (Tripp 1998). In recent years, most SNe Ia cosmological samples are analysed in the SALT2 light-curve framework (Guy et al. 2005, 2007, 2010). The distance modulus μ is corrected for light-curve shape (x_1) and colour (c) as

$$\mu = m - M + \alpha\, x_1 - \beta\, c,$$

where α and β are constants, whose values are determined by fitting to a Hubble–Lemaitre diagram. The colour measurement, c, which corresponds approximately to $E(B - V)$ where the SALT2 template SED is used as reference is thus multiplied by an empirically derived parameter β, the topic of this work. In the SALT2 framework, the absolute magnitude M_B in rest-frame B-band is used as the anchoring point. The SALT2 model performs standardization in a two-step

★ E-mail: rbiswas4@gmail.com (RB); ariel@fysik.su.se (AG)

process. First, the SALT2 model is fitted to the light-curve data of each supernova (SN). These parameters and uncertainties are then used to simultaneously determine the parameters α and β along with the cosmology. Traditionally, this was performed for each cosmological model (and possibly) with complementary data if desired. This made the standardized distance moduli (through the values of α and β) dependent on both the choice of the cosmological model used, and the complementary data. The use of SALT2MU (Marriner et al. 2011), which uses piecewise continuous cosmological distance moduli functions of Λ cold dark matter (ΛCDM) in different redshift bins, ameliorates the cosmological model dependence. More importantly, it paves the way for a generalized intrinsic scatter model in the form of a covariance between the parameters $\{m, x_1, c\}$.

It may be tempting to view the colour–brightness relation as being entirely due to interstellar extinction by dust in the host galaxy of the SNe, i.e. with β corresponding to the total-to-selective extinction parameter, R_B, following the analogy of Milky Way extinction (see e.g. Cardelli, Clayton & Mathis 1989). However, when β is fitted using the ensemble of low- and high-z SNe Ia to minimize the scatter in the Hubble–Lemaitre diagram residuals, its value comes out to be significantly lower than $\beta \sim R_B \approx 4.1$, the Milky Way average value (Astier et al. 2006; Kessler et al. 2009; Amanullah et al. 2010; Suzuki et al. 2012; Betoule et al. 2014; Scolnic et al. 2018). Focusing on the most recent analyses, Betoule et al. (2014) find $\beta = 3.101 \pm 0.075$ based on a sample of 740 SN Ia and Scolnic et al. (2018) find $\beta = 3.030 \pm 0.063$ when they extend the sample with newer discoveries, totalling 1048 SNe with similar light-curve selections. Since only objects with moderate colour have been kept in the samples used for cosmology, $c \leq 0.3$, it has been argued in those studies that the low values of β could be mainly due to intrinsic colour variations (see also Chotard et al. 2011, hereafter C11).

An additional complication to the standardization of SNe Ia magnitudes found over the past decade is that that there is a significant environmental dependence of the distance modulus on the properties of the host galaxy beyond the colour and light-curve shape corrections (Kelly et al. 2010; Lampeitl et al. 2010; Sullivan et al. 2010; Childress et al. 2013; Rigault et al. 2015, 2020; Kelsey et al. 2021). Moreover, it has been realized that selection effects in observational surveys result in incompleteness in the distribution of SNe Ia properties due to interaction with the intrinsic dispersion, and affect the inferred values of β. In cosmological analyses (Kessler et al. 2009; Betoule et al. 2014; Brout et al. 2019) these are usually corrected through a set of bias corrections terms (Mosher et al. 2014; Kessler & Scolnic 2017; Kessler et al. 2019; Popovic et al. 2021) based on simulations. Such simulations require detailed inputs of population models inferred from the data (Kessler et al. 2013; Scolnic & Kessler 2016) and a detailed description of the observational procedure. Given the complexity of such a program and the importance of these parameters to cosmology, complementary checks that do not involve many of such effects like environmental dependence or population models are important cross-checks.

Recently, Brout & Scolnic (2021) suggested that the β is mainly due to dust, but that the extinction properties of SNe Ia depend on the host galaxy stellar mass, thus providing further uncertainty in the reported single 'universal' values of β. Johansson et al. (2021) reach a similar conclusion (but see Thorp et al. 2021, for a different view).

In summary, concerns have been raised that the colour–brightness parameter β derived from cosmological analysis may be biased due to selection effects, procedural mistakes, degeneracies with other parameters in the global fits, redshift uncertainties, K-corrections, calibration errors, and possibly even Milky Way extinction errors. Indeed, over time and for different samples, the reported best-fitting value of β has varied from 1.57 ± 0.15 (Astier et al. 2006), 2.47 ± 0.06 (Suzuki et al. 2012) to $\beta \approx 3.0$, reported by Scolnic et al. (2018). Ideas to reconcile the low values of β with non-standard extinction have been put forward, e.g. that the dimming dust is localized to the circumstellar environment (Wang 2005; Goobar 2008). The latter suggestion has been explored studying the wavelength-dependent attenuation of SN 2014J, a highly reddened SN Ia in the nearby galaxy M82 that also showed non-standard extinction (Amanullah et al. 2014; Foley et al. 2014; Goobar et al. 2014), and through searches of emission from heated circumstellar dust (Maeda et al. 2015; Johansson et al. 2017). The colour relations of samples of nearby reddened SNe Ia have been reporting 'non-standard' extinction laws for over a decade (see e.g. Nobili & Goobar 2008), and have recently been expanded with observations ranging from ultraviolet (UV) to near-infrared (NIR; Burns et al. 2014; Amanullah et al. 2015). The conclusion from these studies is that extinction by circumstellar dust likely plays a minor role in the observed colour–brightness relation of SNe Ia, and that a diverse population of dust in the interstellar medium (ISM) of other galaxies is required to explain the observations, even after intrinsic colour variations are taken into account. An intriguing possibility that has been put forward is that dust grains may be fragmented by collisions between dust clouds, as these are accelerated by radiation pressure from the SN itself (Hoang 2017; Bulla, Goobar & Dhawan 2018), or by radiation in the ISM (Hoang 2021).

While the well-measured nearby SNe Ia, too close to be in the Hubble flow, were able to provide supporting evidence for the 'non-standard' wavelength dependence of attenuation, they could not probe the absolute dimming. This work bridges the efforts between the local and cosmological efforts to study the relation between colour excess and brightness attenuation for SNe Ia. Our measurement of β based on siblings uses the same SALT2 tools as the cosmological analysis, but is free from the potential systematic effects that are often attributed to the Hubble-diagram inferences of β. We emphasize that our analysis is completely agnostic as to the origin of the colour–brightness relation.

2 ZTF AND THE CASE FOR SN IA SIBLINGS

As time domain astronomy surveys get larger and run for longer survey duration, they can find rare objects. Multiple SNe Ia occurring in the same host galaxy, known as siblings. Recent surveys have increased the number of such siblings, allowing ensemble level questions to be addressed through them (Burns et al. 2020; Scolnic et al. 2020), which use the Dark Energy Survey (DES) and Carnegie Supernova Project (CSP) data to discuss to what extent sibling SNe share common properties.

The Zwicky Transient Facility (ZTF) survey (Bellm et al. 2019a; Graham et al. 2019) is a 3π imaging survey of the Northern sky conducted on the (48-inch) Samuel Oschin Telescope at the Palomar Observatory (see Bellm et al. 2019b, for a more detailed description of the survey specifications) between 2018 and 2020, later replaced by ZTF-II. It included a public survey in g and r bands with a nominal 5σ depth of $\sim$20.5 mag with a 3-d cadence, along with a few programs run by the ZTF partnership including an extragalactic survey in the i band with 4-d cadence, designed to obtain a three-filter light-curve sample of SNe Ia for cosmological applications. The procedure for processing the survey data and the data products are described in Masci et al. (2019). As part of the public survey, the Bright Transient Survey (BTS; Fremling et al. 2020) is an effort aimed at collecting an untargeted, nearly complete, magnitude-limited sample of spectroscopically classified transients reaching 18.5 mag.

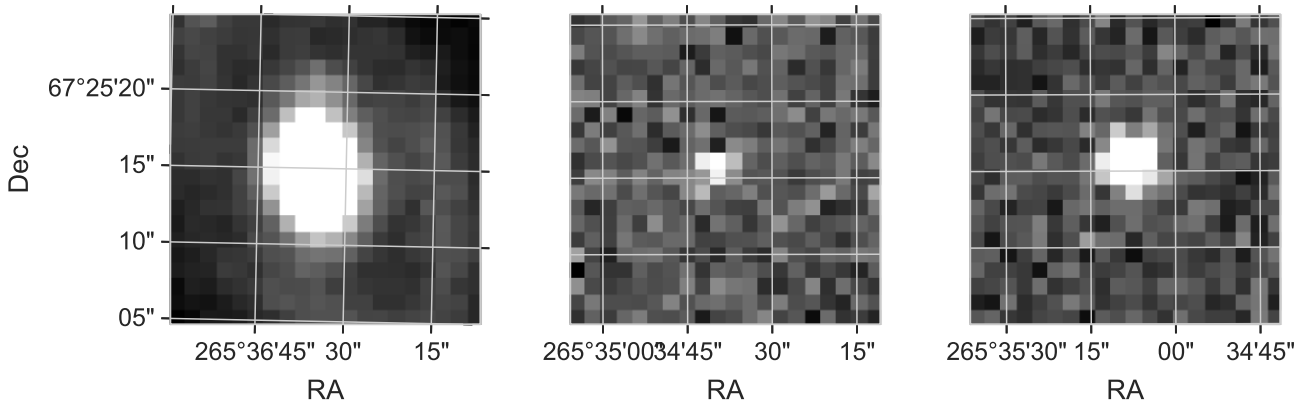

Figure 1. From left to right: *g*-band postage stamps in of the reference image (i.e. the host galaxy) centred at AT 2019lcj, the difference image for AT 2019lcj for the science image on 2019 July 16, and the difference image for SN 2020aewj centred on its position using the science image on 2020 February 7. In both cases, the SNe were close to light-curve maximum.

As ZTF scans the sky with unprecedented speed and depth it has the potential to discover sibling SNe, as discussed in Graham et al. (in preparation) (see also Soraisam, Matheson & Lee 2021, for another reported candidate sibling pair). In this work, we use a particular set of sibling SNe Ia, found at nearly identical positions within a year, but with significantly different observed flux and colours to constrain the parameter β in a cosmology independent way, and yet without any additional assumptions on the origin of the colour excess. Our precision based on this single system is only slightly weaker than constraints obtained analysing $\sim 10^3$ SNe in the Hubble–Lemaitre diagram. This can be improved with a number of sibling SNe, and with different properties of the siblings, can also provide a cosmology-independent constraint on both β and the light-curve width–brightness correction factor, α. Thus, it is a complementary source of information for SN cosmology, and can be also used to probe extinction in these systems even if a wide lever arm in wavelength range is missing.

3 ZTF19AAMBFXC: THE TALE OF TWO SUPERNOVAE

ZTF19aambfxc (Nordin et al. 2019) is a transient detected on the core of a bright galaxy in the public 3-d cadence ZTF survey. It had detections in public alert photometry [signal-to-noise ratio (SNR) $\geq$ 5] from 2019 June 7 through August 14, and the *i*-band Partnership survey from 2019 June 11 and August 23, reaching a brightest observed magnitude of 18.69 in the *r* band. After that, the transient faded below detection. ZTF19aambfxc was reported to Transient Name Server (TNS) as AT 2019lcj. Since it never got as bright as 18.5 mag, the high completeness (93 per cent) threshold reported in the ZTF BTS (Perley et al. 2020), it was, unsurprisingly, not followed up spectroscopically by BTS. Unfortunately, no independent spectroscopic classification has been reported either.

On 2020 January 27, i.e. about 200 d after the detection of AT 2019lcj, an apparent rebrightening of the source occurred, SN 2020aewj, shown in Fig. 1, reaching a significantly brighter state of 17.54 mag in *g* band, well over the BTS classification threshold of 18.5 mag. Upon closer examination, the rebrightening was not at the exact same location as the first detection. The position of the ZTF19aambfxc alerts during this entire period is shown in Fig. 2, with the black markers denoting epochs before Julian Day 245 8800 (2019 November 12), while those after this date are shown in open red squares displaying the positional clustering of alerts during these phases. Visual inspection of the light curve for the alerts during these

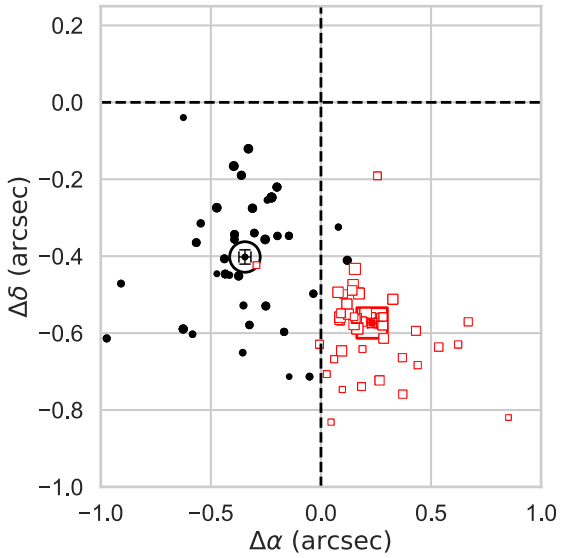

Figure 2. Positions of each alert corresponding to AT 2019lcj (filled black circles) and SN 2020aewj (open red squares) with the size of the markers proportional to the signal-to-noise ratio (SNR) of the alert. The median positions of the alerts corresponding to each SN are highlighted using a large black open circle for AT 2019lcj, while the median position of alerts for SN 2020aewj is highlighted using a large open red square. The intersection of the two dashed lines shows the position of the host galaxy.

two time periods immediately made it evident that there were two distinct explosive transients with a small projected distance between them. While we do not show this light curve (built out of alerts) in the paper, this is also apparent from the forced-photometry light curve shown in Fig. 3 discussed later in this section. The separation between the two transients as shown in Fig. 2 was 0.57 arcsec. Consequently, these transients have been named AT 2019lcj and SN 2020aewj. At the time for the second event, the field was no longer part of the 4-d cadence Partnership *i*-band survey, thus the brighter SN was only observed in *g* and *r* bands.

As part of BTS, the new transient, SN 2020aewj, was securely classified as a normal SN Ia, (Perley et al. 2021) using the Spectrograph for the Rapid Acquisition of Transients (SPRAT; Piascik et al. 2014) on the Liverpool Telescope (LT; Steele et al. 2004). The LT spectrum is shown in Fig. 4, along with a spectrum of the 'typical' normal SN Ia SN 2011fe at a similar phase. However, the older transient must

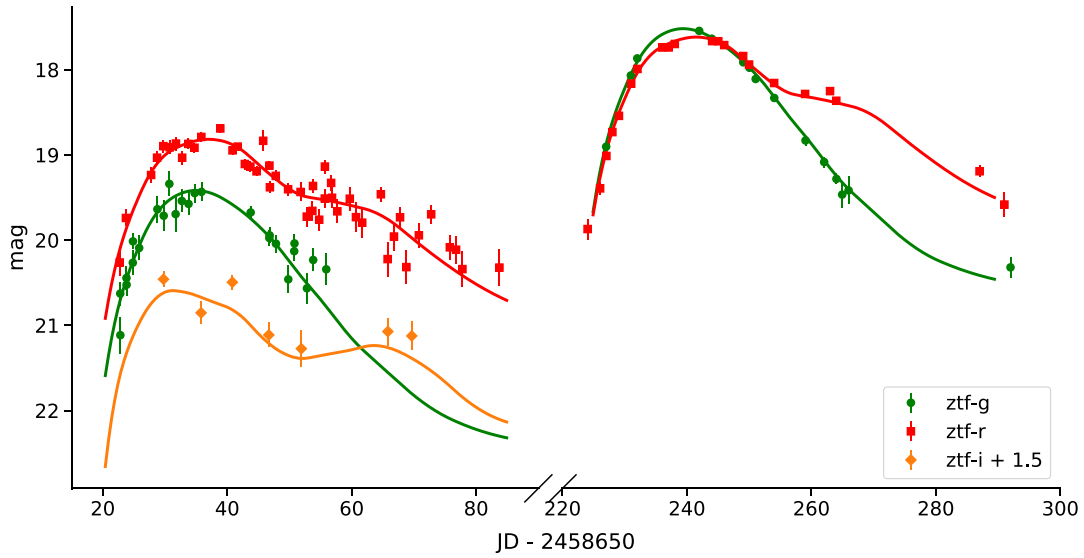

Figure 3. Observations of the sibling system at SNR > 3, in observed bands of the two individual supernovae (SNe) where forced photometry at the location of AT 2019lcj after a Julian Day of 245 8750 has been ignored, while early photometry at the position of SN 2020aewj has been ignored due to contamination. Along with the data, we show the best-fitting SALT2 model curves for each SN Ia. This shows the remarkable coincidence of having two SN Ia within the distance shown in Fig. 2 happen within ∼200 d. The SALT2 parameters and uncertainties corresponding to the best-fitting model and peak brightnesses in the ZTF filters are presented in Table 2, and are different by ∼2 mag in the rest-frame Bessell *B* band.

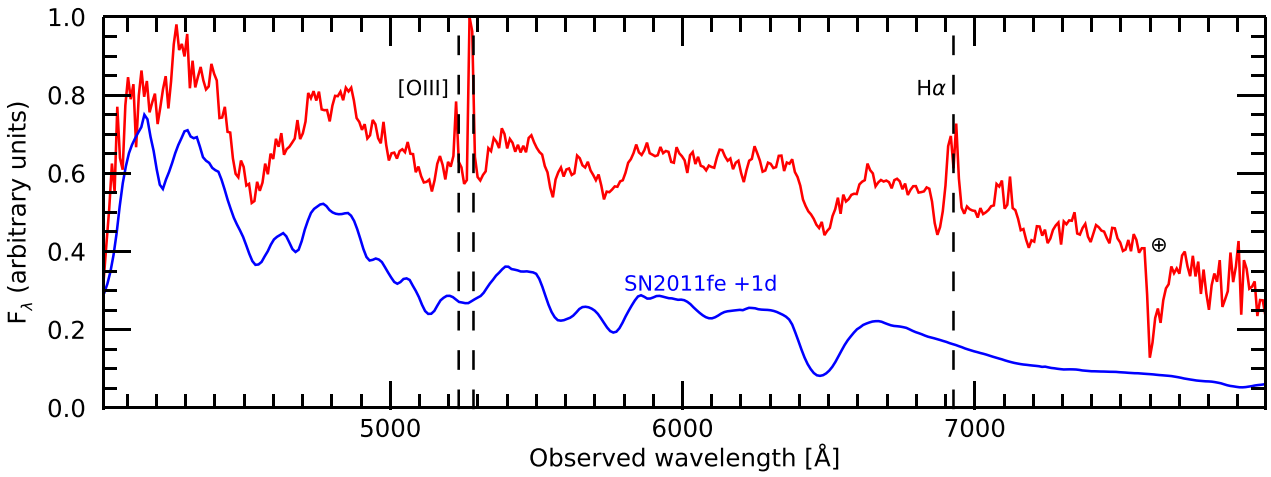

Figure 4. Spectrum of SN 2020aewj obtained at on 2020 February 17 with the Liverpool Telescope (LT). The spectrum was classified as a SN Ia in the Transient Name Server (TNS) classification report (Perley et al. 2021) and provides an approximate redshift of ∼0.055 for the SN. A comparison with a spectrum from SN 2011fe at the same epoch from a compilation by Amanullah et al. (2014) is shown. A more accurate host galaxy redshift, $z = 0.0541$, was measured based on the [O III] and Hα lines, primarily using a spectrum from the Nordic Optical Telescope (NOT), obtained more than 2 months later when the SN had faded.

be photometrically classified. We first describe the photometric light curves and then the host properties.

In the remainder of this section, we first discuss the association of a host galaxy with these two transients. This is followed by a description of the data processing steps needed to obtain a light curve and finally, we use both the host information and the light curves to classify the older transient.

3.1 Data processing of the transient light curves

Using the alert packet from the GROWTH Marshal (Kasliwal et al. 2019) associated with the transient ZTF19aambfxc, we split the observations into two groups assigning them to AT 2019lcj if the Julian Day of the observation, JD ≤ 245 8800 (2019 November 12), and SN 2020aewj otherwise. The time of the split was determined by visual inspection. We determined the position of each SN, by taking the median of the positions of the 5σ detections for each SN. These locations are summarized in Table 1, and the positions of these detections are shown in Fig. 2.

We run forced photometry at these SN locations using a pipeline, hereafter known as the ZUDS pipeline[1] (Dhawan et al. 2021), which

[1] https://github.com/zuds-survey/zuds-pipeline

Table 1. Positions of the two SNe AT 2019lcj and SN 2020aewj separated by 0.57 arcsec at $z = 0.0541$.

ID	RA (°)	Dec. (°)	Host sep (arcsec)
AT 2019lcj	265.42935	67.96189	0.50
SN 2020aewj	265.42974	67.96183	0.42

performs aperture photometry using the ASTROPY affiliated package PHOTUTILS (Bradley et al. 2019), using a 6-pixel diameter aperture on the difference images. The reference images for the difference images are constructed by co-adding exposures from epochs at least 30 d or more before the initial estimate of the time of maximum from the alert photometry, using the software SWARP (Bertin 2010). In order to build the co-add, we only take epochs with seeing between 1.7 and 3 arcsec and a magnitude limit deeper than 19.2 mag. For consistency, we use the same reference image for both SNe. In the ZUDS pipeline, difference images are obtained using HOTPANTS (Becker 2015), an implementation of the image subtraction algorithm (Alard & Lupton 1998). The zero points for each epoch are computed by the Infrared Processing and Analysis Center (IPAC), corrected for a 6-pixel diameter aperture. For the *i* band, we use the images corrected for an observed fringing pattern, using the FRINGEZ software (Medford et al. 2021). From the IPAC forced-photometry service (Masci et al. 2019) at the same locations, we obtain the metadata for each observation, including the magnitude limit $m_{\rm lim}$ of the observation, the seeing of the observation, and the standard deviation $\sigma_{\rm pix}$ on the background at the pixel on which the SN is located. We combine this information with the ZUDS pipeline results for data quality assessment. Specifically, we only use those observations that satisfy the following conditions: $1.0 <$ seeing < 4.0 arcsec, $m_{\rm lim} < 19.2$ mag, and $\sigma_{\rm pix} < 14.0$, where $\sigma_{\rm pix}$ is the robust σ per pixel in the science image and is used as a metric to remove non-photometric data. We then use a maximum likelihood method to fit the SALT2 model to each of these two SN light curves. The low seeing values are removed to protect against undersampling during image subtraction. We then remove the epochs that have 5σ flux outliers relative to the best-fitting SALT2 model (discussed later and summarized in Table 2) and use the remaining selected points as the light curves of the individual SNe. The final photometry data sets used are included as Tables C1 and C2. The resulting light curves are shown in Fig. 3. As stated earlier, this light curve clearly shows the presence of two transients with no detections for a period of over 100 d in between. For the unclassified transient AT 2019lcj, we notice that AT 2019lcj has a shoulder in the redder bands (*r*- and *i* band) as seen in Fig. 3 strongly indicating that the SN is of Type Ia. We will verify this shortly after discussing its redshifts and host properties.

3.1.1 *Host association and properties*

The top panel of Fig. 5 shows the positions of the SNe and the two nearest galaxies. Both SNe are found to lie on the core of a galaxy, while there is a second nearby galaxy, approximately 30 arcsec away that we deem extremely unlikely to be the host of any of the two SNe. We will refer to the first galaxy as the host galaxy. A high SNR spectrum from the Alhambra Faint Object Spectrograph and Camera (ALFOSC) instrument on the Nordic Optical Telescope (NOT)[2] taken on 2020 April 28 was used to determine the properties of the galaxy. The host galaxy redshift was accurately measured to be $z = 0.0541$ from the position of [O III] and Hα lines, in excellent agreement with the best fit to the SN spectrum of SN 2020aewj ∼0.055. This late spectrum is available from the authors upon request. The angular distances along with the absence of a nearby galaxy establish the two transients as siblings, i.e. have the same host galaxy. Additionally, the spectrum from the host provides us with an accurate measurement of their common redshift, used in the calculations later.

While the two conclusions above are central to this paper, we expand our study of the properties of the host galaxy as it might be relevant to the conclusions on extinction. We retrieve the science-ready co-added images from the Sloan Digital Sky Survey Data Release 9 (SDSS DR 9; Ahn et al. 2012), the Panoramic Survey Telescope and Rapid Response System (Pan-STARRS, PS1) DR1 (Chambers et al. 2016), the Two Micron All Sky Survey (2MASS; Skrutskie et al. 2006), and pre-processed *Wide-field Infrared Survey Explorer* (*WISE*) images (Wright et al. 2010) from the unWISE archive (Lang 2014).[3] The unWISE images are based on the public WISE data and include images from the ongoing NEOWISE Reactivation mission R3 (Mainzer et al. 2014; Meisner, Lang & Schlegel 2017). We use the software package Lambda Adaptive Multi-Band Deblending Algorithm in R (LAMBDAR; Wright et al. 2016), which is based on a software package written by Bourne et al. (2012) and tools presented in Schulze et al. (2021), to measure the brightness of the host galaxy. The spectral energy distribution (SED) was modelled with the software package PROSPECTOR[4] version 0.3 (Leja et al. 2017). We assumed a linear–exponential star formation history, the Chabrier (2003) initial mass function (IMF), the Calzetti et al. (2000) attenuation model, and the Byler et al. (2017) model for the ionized gas contribution. The priors were set as described in Schulze et al. (2021).

The best-fitting host galaxy SED, along with its parameters, is shown in the lower panel of Fig. 5. This shows that the stellar mass of the galaxy is $\sim 10^{10.48^{+0.11}_{-0.46}}$ M$_\odot$. This is approximately equal to the threshold usually chosen to divide SN Ia samples into two groups to which different corrections are applied. Fortunately, this will not have an impact on our calculations that depend on the difference of the distance moduli of the pair as the pair share the same host galaxy. We also note that the measured stellar mass is very comparable to the Milky Way value reported by Licquia & Newman (2015), thus the dust properties of this host galaxy are expected to be similar to the Milky Way, even in a model like Brout & Scolnic (2021).

3.1.2 *Photometric classification of the AT 2019lcj*

To verify the SN Ia class suspected from the light-curve shape, we classify the type from the photometry. Aside from the light-curve shape, we note that the SN is 2 mag dimmer than expected of a SN Ia in the same galaxy as demonstrated by SN 2020aewj. Additionally, the stretch x_1 of the AT 2019lcj is found to be 0.54 ± 0.18. Thus we limit the comparison to models of dimmer SNe like core-collapse SNe and peculiar SNe like 1991bg-like SNe, while excluding overluminous peculiar types like 1991T on the basis of the peak brightnesses and the stretch. The maximum likelihood fit to the light curve in Fig. 3 with models of different SN classes and subtypes. Since the models considered have different numbers of parameters and are non-nested, we cannot use the likelihood ratio test to compare the models. Rather than computing the Bayesian

[2]PI: Sollerman and Goobar.

[3]http://unwise.me

[4]https://github.com/bd-j/prospector

Table 2. Properties of the two SNe AT 2019lcj and SN 2020aewj: The SALT2 parameters of the SNe based on a maximum likelihood fit, along with the synthetic peak magnitudes for this best-fitting model in the ZTF *g*-, *r*-, and *i* band along with the Bessell *B* band.

ID	t_0 (d)	$10^4 \times x_0$	x_1	c	*g* peak (mag)	*r* peak (mag)	*i* peak (mag)	*B* peak (mag)
AT 2019lcj	245 8685.41 ± 0.15	2.67 ± 0.12	0.54 ± 0.18	0.57 ± 0.04	19.4	18.8	19.1	19.7
SN 2020aewj	245 8889.92 ± 0.08	17.08 ± 0.56	0.61 ± 0.13	0.00 ± 0.03	17.5	17.6	18.2	17.6

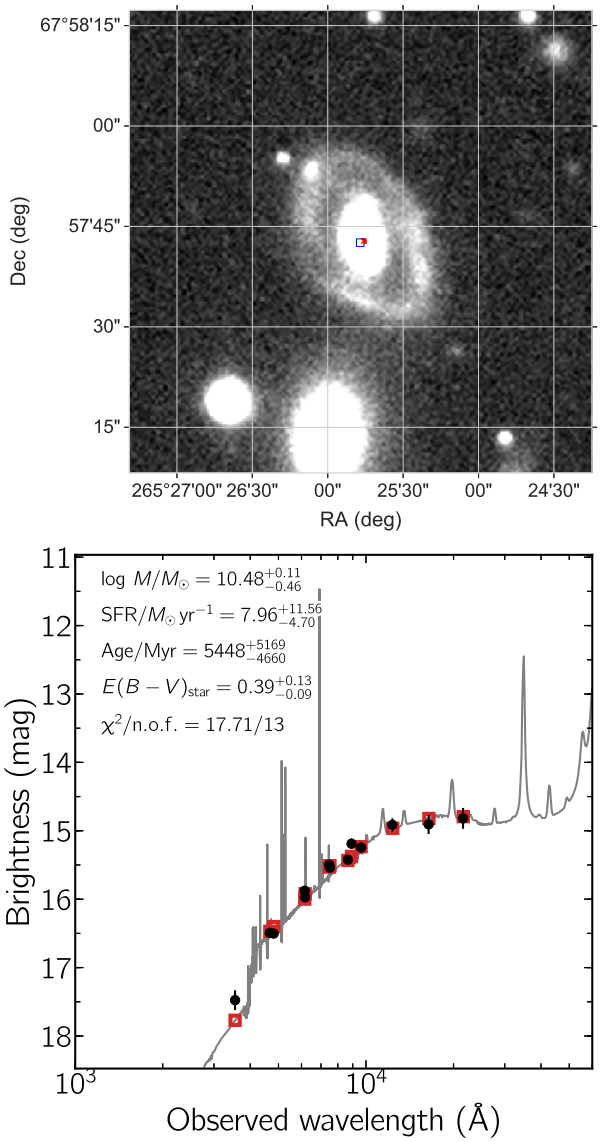

Figure 5. Host association and properties. Top panel: location of nearby galaxies obtained from the Legacy Survey in *g* band from the National Optical Astronomy Observatory (NOAO) data lab is shown along with the SNe. The location of AT 2019lcj is indicated with a red cross, while SN 2020aewj is shown with a blue open square almost spatially coincident in the core of the host galaxy. Bottom panel: the best-fitting model spectral energy distribution (SED) of the host galaxy of ZTF19aambfxc (photometric observations •, model-predicted magnitudes □) from multiband photometry. The solid line displays the best-fitting model of the SED. The fitting parameters are shown in the upper left-hand corner. The abbreviation n.o.f. stands for numbers of filters.

Table 3. Bayesian information criterion (BIC) of different SN types fitted to the multiband photometry of AT 2019lcj shown in Fig. 3.

SN type	BIC	ΔBIC
SN Ia: Norm	419.47	0
SN Ia: 91bg	1200.22	780.75
SN Ibc	1042.55	623.08

evidence for each model that is computationally expensive, and the population priors are likely not well known, we use the Bayesian information criterion (BIC; Schwarz 1978) for each model, which for Gaussian-distributed deviations amounts to

$$\mathrm{BIC} = -2\log(L_{\max}) + k\log(n), \quad (1)$$

where $L_{\max}$ is the maximum of the log likelihood, n is the number of data points, and k is the number of parameters in the model. The difference in BIC values between two models is approximately proportional to the logarithm of the Bayes ratio of the two models, with $\Delta\mathrm{BIC} = 10$ considered decisive evidence against the model with higher BIC (Liddle 2007). Applying a maximum likelihood fit to different kinds of templates of SNe types, we calculate the BIC values as shown in Table 3. We choose the SN Ib/c template kindly provided Peter Nugent[5] and the *K*-correction estimates in Nugent, Kim & Perlmutter (2002). Since the observed colours of the SN are red, we also fit the SN1991bg template from Nugent et al. (2002). The column ΔBIC has values of BIC(model) − BIC(SALT2). Thus models considered here with $\Delta\mathrm{BIC} \gg 10$ are decisively disfavoured. Thus, the entries in Table 3 show that from the photometric data alone, we can say that of the types of SNe and templates considered, AT 2019lcj is a normal SN Ia.

4 METHOD

Sibling SNe are inferred to be in the same galaxy through their transverse proximity, and thus have virtually identical (radial) distance. First, we quantify the potential difference in the radial distance in comparison to the intrinsic dispersion of SN Ia. Galaxies are typically of size ∼kpc, and host SN Ia within a few tens of kpc from the centre of the galaxy (Galbany et al. 2012; Gagliano et al. 2021). Thus, sibling SNe are expected to have a distance difference $\delta d \lesssim 100$ kpc, resulting in a distance modulus difference of $5/\ln(10) \times \frac{\delta d}{d}$. For a sibling at a redshift of $z = 0.0541$, even for a distance difference of ∼100 kpc this difference is $\approx 10^{-3}$ which is two orders of magnitude smaller than the distance uncertainty induced by the intrinsic dispersion of $\sigma_{\rm int} \sim 0.1$ of SN Ia. This understanding can be expressed as a prior probability that is a normal distribution in the difference of the distance moduli with a standard deviation related to the intrinsic dispersion:

$$\Pi(\Delta\mu|\mathcal{H}) = \mathcal{N}(\Delta\mu, \sigma^2). \quad (2)$$

[5]https://c3.lbl.gov/nugent/nugent_templates.html

In this work, we assume the SALT2 model with an intrinsic dispersion affecting the brightness of SN Ia coherently at all wavelengths (technically following the Guy et al. 2010, hereafter G10, intrinsic dispersion). This means that the estimated distance modulus of a SN can be normally distributed about the true distance modulus with a standard deviation of $\sigma_{\rm int}$. The value of the intrinsic dispersion in SN samples is determined for each sample, and is generally $\sim$0.1 mag. The intrinsic dispersion of SN Ia in the same galaxy (or equivalently if sibling SNe have correlated intrinsic scatter) has been investigated (Burns et al. 2020; Scolnic et al. 2020) and found to be consistent with low correlations r. Thus, we choose the standard deviation in our prior probability to be $\sigma^2 = 2\sigma_{\rm int}^2(1-r)$, with a fiducial value of $r = 0$. We also use the SALT standardization relation (Tripp & Branch 1999) as used in recent SN cosmology analyses (Betoule et al. 2014; Jones et al. 2018a; Scolnic et al. 2018; Brout et al. 2019; Hinton et al. 2019):

$$\mu_i = m^\star_{B\ i} + \alpha\, x_{1i} - \beta\, c_i - M^\star_B + \delta_{{\rm Host}_i,{\rm loc}_i}\mu, \tag{3}$$

where, for completeness, we have included a correction term for (potentially local) environment dependence. The term involving the impact of the host galaxy has been mostly used in the SN cosmology literature as a step function involving the global properties of the host galaxy such as stellar mass $M^{\rm Host}_{\rm stellar}$, as in $\delta_{\rm Host,loc}\mu = {\rm step} \times (M^{\rm Host}_{\rm stellar} - M_{\rm thresh})$, where step $\sim$ 0.1 mag and $M_{\rm thresh} \sim 1 \times 10^{10}\,{\rm M}_\odot$ are obtained by minimizing the Hubble residuals from a fiducial model. For such a model where the environmental dependence is through global properties of the host, clearly this difference disappears for SN siblings. However, such environmental dependence is expected to depend on the local properties of the galaxy. For example, this may be driven by the properties of the progenitor(s) that inherited the properties of the local stellar population or due to dust that could also be local. This could have important consequences for the measurements of H_0 (Rigault et al. 2015, 2020), though the details are part of a current debate (Jones et al. 2018b). Thus, these siblings, even though separated by a tiny projected distance, could be further apart in the galaxy (radially) and have different properties. Nevertheless, as far as estimated corrections go, corrections from local properties are made by analyses restricted by projected distances, often in regions of projected distances of $\sim$2 kpc. The siblings being 0.6 kpc (using a *Planck* cosmology (Planck Collaboration VI 2020)) apart are close enough that any correction term due to local measurements would also be extremely similar for the two SNe Ia and thus the difference would be small. Thus, we set $\delta_{\rm Host,\ loc}$ to 0 in the rest of this work.

Thus, for a pair of sibling SNe, we get

$$\begin{aligned}\Delta\mu \equiv \mu_1 - \mu_2 &= -2.5\log(x_{01}/x_{02}) \\ &\quad + \alpha\,(x_{11} - x_{12}) - \beta\,(c_1 - c_2),\end{aligned} \tag{4}$$

where we have used the approximation $m^\star_B = -2.5 \times \log 10(x_0) + K$, where K is a constant.

In this model, the parameters are $\Psi = \{\psi, \phi_1, \phi_2\}$, where the SALT2 model parameters for each SN are $\phi \equiv \{x_0, x_1, c\}$, and the subscripts 1 and 2 refer to the two SNe, and $\psi \equiv \{\alpha, \beta\}$. We can write the posterior distribution $P(\Psi|D, \mathcal{H})$ on Ψ, where D is the photometric data, along with spectroscopic data needed to determine the redshift z, and $\mathcal{H}$ represents our understanding of the astrophysics leading to the equations we use:

$$\begin{aligned}P(\Psi|D,\mathcal{H}) &\propto P(D|\Psi,\mathcal{H})\Pi(\Psi|\mathcal{H}) \\ &= P(d_1|\phi_1,\mathcal{H})P(d_2|\phi_2,\mathcal{H})\Pi(\Psi|\mathcal{H}), \\ \Pi(\Psi|\mathcal{H}) &= (\mathcal{N}(\mu_1 - \mu_2, \sigma^2)\Pi(\alpha)\Pi(\{\beta, \phi_1\,\phi_2\,\}),\end{aligned} \tag{5}$$

where $P(D|\Psi,\mathcal{H})$ is the likelihood function of Ψ, and $\Pi(\Psi|\mathcal{H})$ is the prior on Ψ. Utilizing the fact that the time of peak of the SNe is reasonably well constrained, and the flux due of AT 2019lcj is negligible at the time of SN 2020aewj that peaks 205 d after AT 2019lcj, factorizing the likelihood function into independent likelihood functions for the data of AT 2019lcj and SN 2020aewj is an excellent approximation. Therefore, we write this as the product of individual likelihood functions $P(d_i|\phi_i, \mathcal{H})$ is the likelihood function of the SALT2 model parameters for the ith SN. This model for the SN photometry includes the impact of Milky Way extinction by multiplying the SALT SEDs by a time-independent, wavelength-dependent extinction calculated using the fitting functions of Cardelli et al. (1989) with the $E(B-V)$ value for Milky Way at the location of the SNe evaluated using the recalibration (Schlafly & Finkbeiner 2011) of the Schlegel, Finkbeiner & Davis (1998) dust maps. Finally, the likelihood function encodes the assumption that the measured fluxes are Gaussian distributed about the SALT2 model fluxes with variances described by the flux uncertainties reported in the photometry, as well as the uncertainties on the model as determined from SALT2 training. The prior $\Pi(\Psi|\mathcal{H})$ includes chosen priors on each of the parameters $\Pi(\alpha)\Pi(\beta\,\phi_1\,\phi_2)$. Our chosen priors on each parameter in Ψ in this paper are uninformative (uniform, hard priors) except for α for which we sometimes adopt the Pantheon result (Scolnic et al. 2018), as described as part of each calculation in Section 5. Aside from these choices, we use the result of a different measurement (galaxy association) affirming that these SN Ia are siblings, to further constrain these parameters, expressed as the normal distribution equation (2) using equation (4) for $\Delta\mu$. We use EMCEE (Foreman-Mackey et al. 2013) to explore the parameter space.

5 RESULTS

5.1 Constraints on β

Having confirmed that the siblings are SNe Ia, we employ the methodology discussed in Section 4 to calculate the posterior distribution of all the parameters Ψ based on the data from the siblings in Fig. 6. We take into account the spatial coincidence of this sibling pair, thereby using equation (4) and calculate the posteriors using equation (5). In Fig. 6, the blue contours enclose 68 per cent and 95 per cent of the probability, while the dashed black lines show the maximum likelihood estimates of the parameters from each of the single SN. Uninformative uniform box priors were used as hard priors on all of the parameters except α where a Gaussian prior of 0.15 ± 0.01 incorporating the values obtained in the analysis of the Pantheon data set (Scolnic et al. 2018) was used. The constraints on the parameter α effectively stems entirely from the Pantheon prior. The excellent match between the maximum likelihood estimates of the individual SNe in Table 2 (with no knowledge of the sibling nature) and the posteriors of the joint likelihood confirm the expected result that SALT2 parameters of individual SNe are not affected by the global parameters like α and β. Thus, the only new information from the sibling nature is the constraints on β that would be entirely unconstrained from the individual fits of two SNe.

5.2 Consistency of β constraints with previously reported values

Therefore, we focus on the constraints on β from this system. In Fig. 7, we show the posterior probability density function (PDF) on β inferred from the sibling SN system, when marginalized over all other parameters in Ψ, and using the Pantheon prior on α. The constraints are 3.5 ± 0.3 that is an 8 per cent measurement on the parameter β from this system alone. This can be compared to

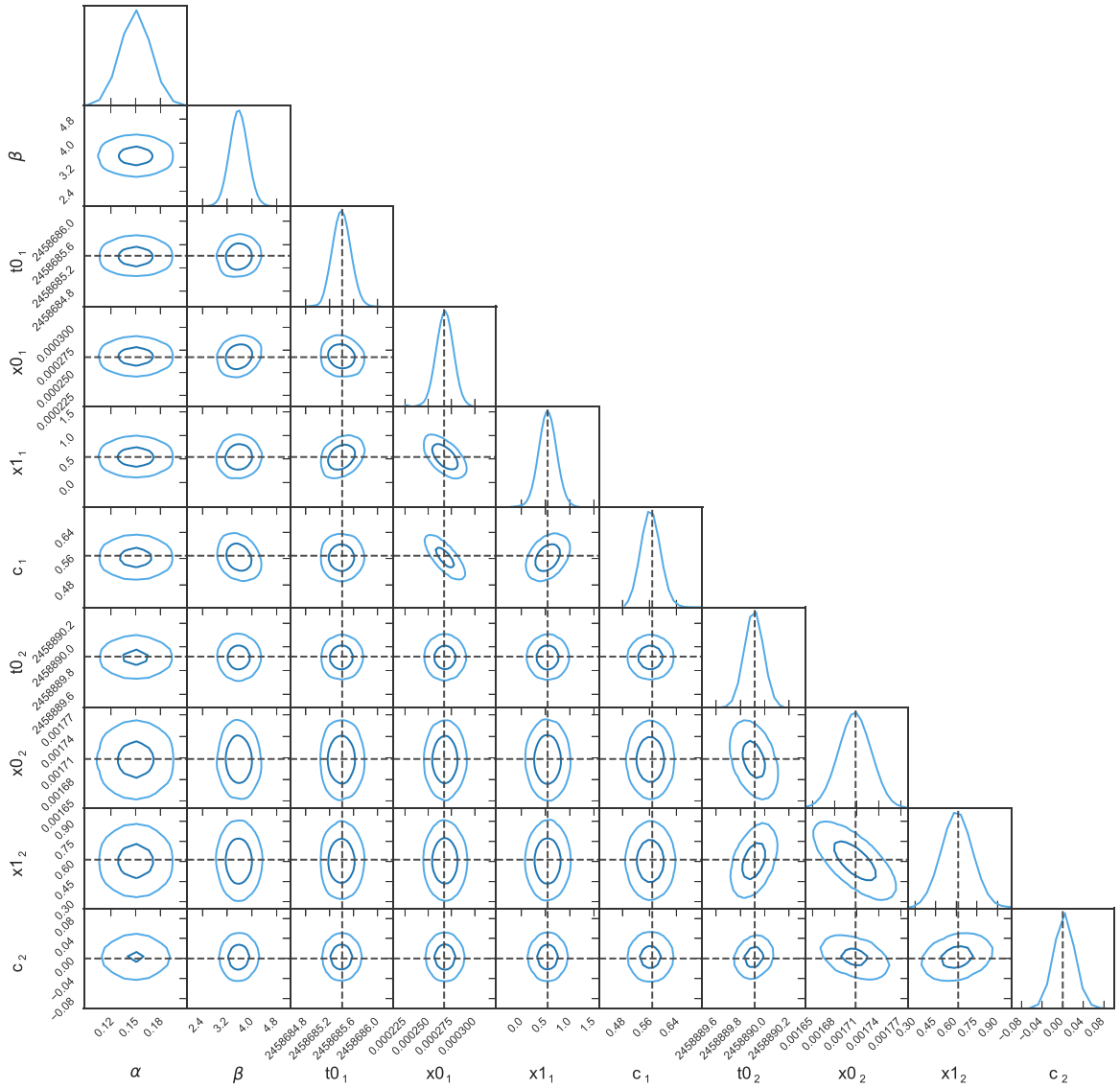

Figure 6. The joint posterior distribution of the SALT2 light-curve parameters for the two SNe and the global parameters α and β. The contours enclose 68 per cent and 95 per cent of the probability, while the dashed lines show the maximum likelihood estimates of the parameters shown in Table 2 if available from each of the single SNe. Uninformative uniform box priors were used as hard priors on all of the parameters except α where a Gaussian prior of 0.15 ± 0.01 was used incorporating the values obtained in the analysis of the Pantheon data set (Scolnic et al. 2018).

constraints on β from cosmological surveys, in terms of consistency of values summarized in Table 2 and the magnitude of uncertainty. SN cosmology survey results in the past decade using the SALT2 model include the Joint Light Curve Analysis (JLA; Betoule et al. 2014), the results on the Pantheon sample (Jones et al. 2018a; Scolnic et al. 2018) from PanSTARRS and the DES (Brout et al. 2019). All of these surveys presented results with the G10 and the C11 intrinsic scatter models. Of these the JLA studied the constraints on α, β based on different cosmological models, and the use of complementary information from cosmic microwave background and galaxy surveys, while the other studies presented cosmological model insensitive constraints using SALT2MU. For the G10 scatter model, JLA reported values of β between 3.099 and 3.126 with an uncertainty of $\sim$0.075–0.1, while the DES/PanSTARRS analysis obtains a slightly lower value 3.02–3.03 with an uncertainty of $\sim$0.11–0.13. The values with a C11 intrinsic scatter model based on the Nearby Supernova Factory (SNFactory) studies are consistently higher, ranging from 3.27 to 3.4 with a similar uncertainty $\sim$0.1, while the values obtained from DES and PanSTARRS range from 3.51 to 3.61 with the uncertainties of the order 0.15–0.25. Clearly the values here are very consistent with C11 intrinsic scatter model values reported from past surveys, while the consistency with G10 scatter model based analyses is at the level of $<2\sigma$. Finally, we show the comparison with a determination of β from 69 low-redshift SN Ia (Dettman et al. 2021) from the Foundation Supernova Survey (Foley et al. 2018).

5.3 Impact of priors and assumptions

In this work, we do not estimate the intrinsic dispersion as is customary in SN cosmology analysis. Instead, we posit that the magnitude of intrinsic dispersion is 0.1 based on results from previous surveys. Therefore, in Fig. 8, we study the impact of

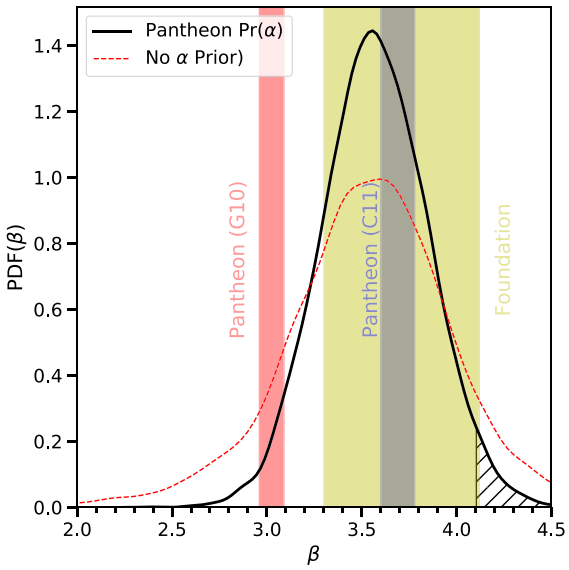

Figure 7. The probability density function (PDF) of β marginalized over all other model parameters is shown in solid (dashed) black (red) curve for an intrinsic scatter of 0.1 and correlation $r = 0$, with (without) the Pantheon priors on α. The constraints are $\beta = 3.4\ (3.6) \pm 0.3\ (0.4)$. The shaded vertical rectangles show the 1σ constraint on β from the PanSTARRS spectroscopic sample (Scolnic et al. 2018) for the G10 model of intrinsic scatter (red) and the C11 model (blue) and for 69 low-redshift SN Ia from the Foundation Supernova Survey (yellow) (Dettman et al. 2021). The hatched black region shows the probability of the β value being at least as large as the value expected if the colour-dependent extinction was solely due to interstellar medium (ISM) host dust of the same nature as the Milky Way. This probability associated with this region is 2.5 per cent.

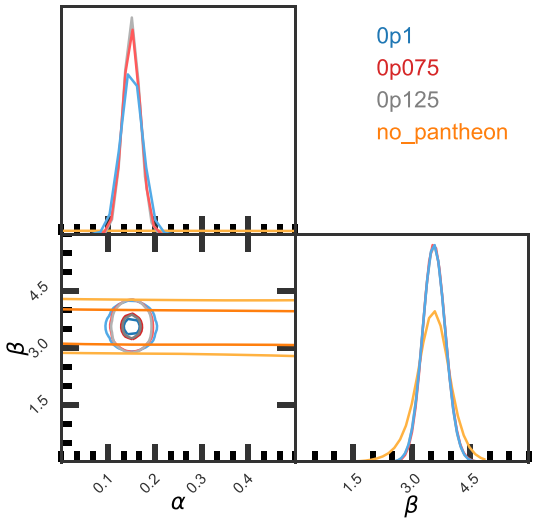

Figure 8. Joint constraints on α and β from the SN Ia sibling system when the magnitude of intrinsic dispersion used in calculating the posterior is varied from the fiducial value of 0.1 (blue) to 0.075 (red) and 0.125 (grey). Finally, the orange contours show the results for the fiducial choice of $\sigma_{\rm int} = 0.1$ when the Pantheon priors on α are not used. This leaves α completely unconstrained, but the constraints on β only change slightly from 3.4 ± 0.3 to 3.6 ± 0.44.

constraints on α and β as we vary the magnitude of the intrinsic dispersion. Fig. 8 shows the constraints on α and β for the fiducial case (shown in Fig. 6) of $\sigma_{\rm int} = 0.1$ (blue) and two additional cases: $\sigma_{\rm int} = 0.075$ (red) and $\sigma_{\rm int} = 0.125$ (grey). Within this small range of changes to the assumed values of intrinsic dispersion, the constraints on β are unaffected. Finally, this figure also explores the impact of not using the Pantheon data set to put a prior on α (orange). We find that removing this prior leaves α entirely unconstrained but the constraints on β only change modestly from $\beta = 3.4 \pm 0.3$ to 3.6 ± 0.4. We can understand this insensitivity as arising from the peculiarities of the sibling system: the x_1 values of the two SN Ia have virtually the same value, while the difference in c is large. This leads to a very tiny dependence on α in equation (4), and consequently has small effects on the constraints on β. The downside of this same peculiarity is that without priors, the constraints on α are extremely weak as shown in Fig. 8.

5.4 Comparison with Milky Way R_B

Data-driven models like SALT2 do not require any physical interpretation to parameters like β, but as a best-fitting value to the SALT standardization relation for a sample of SNe Ia. However, the colour excess (after correction for Milky Way reddening) is interpreted in other models (see e.g. Tripp & Branch 1999) as dust extinction in the host galaxy and is described by a fitting function dependent on the total-to-selective extinction ratio R_V (Cardelli et al. 1989), or in the rest-frame B band, $R_B = R_V + 1$. In such models, one cannot exclude different values of R_V in each galaxy, describing the size and composition of the dust–grain population in the host galaxy ISM along the line of sight. Such a measurement of R_V in diverse populations of galaxies is poorly known, but is well measured in the Milky Way, where it varies with direction and has an average value of $R_V = 3.1$. Using the Tripp (1998) relation, one may expect that the value β is related to the R_V for extinction as $\beta \approx R_B$. SN surveys (as discussed above) usually obtain values of β consistent with $R_V \approx 2$, well below the average Milky Way value, but cannot probe the distribution or variance of R_V. This can be done using longer lever arms in colour (see e.g. Amanullah et al. 2015, and references therein). In this work we show that one can also extract it from galaxies that host SN siblings, as the β value inferred here is specific to the host galaxy. The R_V value implied by our constraints is similar $\sim$2.5, and the probability of the implied R_V value being at least as large as the average Milky Way value has a total associated probability of 2.5 per cent. We note, however, that deviations from the 'standard' dust law have also been reported in Galactic studies (see e.g. Nataf et al. 2016).

Since this determination of R_V is model dependent, we study this in other models as well. First, as a consistency check, we also compute the total-to-selective absorption ratio, R_V, using the SN Ia model in SNOOPY (Burns et al. 2011). SNOOPY fits the host galaxy R_V and colour excess, $E(B - V)$, using templates based on the colour–stretch parameter, S_{BV} (Burns et al. 2014). We present details of the inference procedure in Appendix A, but summarize the results $R_V \sim 2.8$. Finally, we also look at the more general dust model from Brout & Scolnic (2021) in Appendix B. In this model, the colour of a SN Ia as determined by SALT2 is postulated to be a linear combination of reddening due to dust in the host galaxy, and colour of the SN with respect to a template with coefficients R_B and β. Thus, there are two colour laws in this model, and more free parameters compared to the traditional SALT2 model. The parameter β in this model is not directly related to R_B. While we postpone a more complete uncertainty analysis to future work, we show that the sibling system can be used to probe such models. For example,

it suggests that if R_V is 3.1 (the host galaxy of these siblings has a similar stellar mass as the Milky Way), we can show that this suggest a difference in $c_{\rm int}$ of $\gtrsim$3, which is much larger than the standard deviation of the Gaussian distribution for individual SN, which is ameliorated for a lower R_V and low values of β. Therefore, in multiple models, this sibling pair suggests that the host galaxy has a lower value of R_V than the Milky Way.

5.5 Uncertainty and future prospects

As discussed earlier, the uncertainty on β obtained from cosmological surveys in the last decade depends on the intrinsic scatter model used, and range from 0.075 to 0.15 for the G10 model, and 0.15 to 0.25 using the C11 model. These surveys use a large number of SN Ia for example 740 in JLA, 207 in DES, 1048 in the Pantheon sample, 1364 in the photometric PanSTARRS analysis to obtain such constraints, and are tighter than the constraints from this single system by a factor of 2–3. For constraints from sibling SNe to be useful in understanding distance modulus bias, it is important for these constraints to be competitive, which is possible by combining the results from a number of SN Ia siblings. Currently, ZTF has a few SN Ia siblings (see Graham et al., in preparation), while data collection continues in phase II. DES has published a few siblings, and one can expect more siblings from large ongoing surveys like ZTF, Young Supernova Experiment (YSE; Jones et al. 2021), and upcoming surveys like the Legacy Survey of Space and Time (LSST; LSST Science Collaboration 2009; Ivezić et al. 2019) at the Vera C. Rubin Observatory. While a simple square root of N calculation would suggest that $\sim$10 sibling systems should tighten the constraints to competitive levels, this actually depends on the properties of the SN Ia themselves.

6 DISCUSSION

In this paper, we have exploited the fact that the distance moduli of two SNe in the same galaxy are virtually identical and any radial difference is much smaller than the impact from intrinsic dispersion. We quantify this at the beginning of Section 4. This property of multiple distance measures in the same galaxy is also the principle used to transfer distance measurements from other calibrators in building the local distance ladder. We use this fact to study the standardization procedure used in SN cosmology using the SALT standardization relation, as well as shed light on the physical processes underlying the colour–luminosity part of the relation.

The sibling pair under consideration has certain special properties that allow us to evade several systematics. These properties will not hold for siblings in general and so we discuss these.

First, this sibling pair has an extremely small angular separation (0.57 arcsec) corresponding to a projected distance of 0.6 kpc. The angular separation is smaller than the scale at which the dust maps of the Milky Way appreciably vary, and thus the Milky way extinction, which is not perfectly known affects them in an identical way, further reducing potential systematic uncertainties. An often discussed issue with such distance measurements for SN Ia is the impact of the environment through local and global properties of the host galaxy. The local impacts are sometimes corrected for using host properties that are local to the line of sight. Despite the coincidental projected proximity, the pair of siblings under consideration may be still be physically affected by such environments due to a larger distance along the line of sight. However, the correction terms, which must be based on the projected local properties, must be zero in our particular example, as discussed in Section 5 enabling us to emulate the results incorporating such corrections without determining the local host properties. For more generic cases of SN Ia siblings, we are unlikely to repeat such proximity, and differences in SN Ia distances might need to take into account the differences in local stellar populations. While that would complicate the computation we did for other cases, this could also potentially help in resolving the difference between local and global dependence on galaxy properties.

A second special property is the similarity of the light-curve shape parameter x_1 and difference in the colour parameter c of the sibling SNe, which drives the strength of our constraints on β and the relative insensitivity on α. In general, for individual pairs of sibling SNe, we will not get as tight constraints on β, and there might be higher sensitivity to the priors on α. On the other hand, samples of sibling SNe that would have a distribution of differences in parameters should enable using the same method to put tighter constraints on these parameters.

Finally, we note that the two SNe siblings may be found using different instruments (for e.g. in different surveys). In our case, we have been fortunate to obtain this sibling pair using the same instrument and thus our work is independent of interinstrumental systematics

7 CONCLUSIONS

Standardization of SN Ia and the characterization of systematic uncertainties in the process remains a crucial piece of SN cosmology and its application to constraining the phenomenology of dark energy and the Hubble tension. Such systematics are particularly important when using SN samples promised by ongoing and upcoming surveys where the large SN sample size is expected to reduce the statistical uncertainties. Within the current industry standard of standardization based on the SALT2 model, an important aspect is the determination of population level parameter α, β that determine the linear importance of light-curve shape and colour of SN Ia relative to their observed brightness in the standardization process. In the conventional process, this determination of α, β can depend on the cosmological models used, the contribution due to environmental effects, and the Malmquist bias of the survey sample relative to the training sample. The estimates are often corrected for using catalogue simulations that forward model entire surveys and their selection function using input populations of SN Ia that are inferred from data. This is a complex process. Hence complementary and independent information determining these parameters would be extremely useful.

In this work, we use the fact that the difference in distances to sibling SNe is negligible, to address standardization in a way that is independent of cosmology and several other systematics such as possible correlations of SN brightnesses with local or global host galaxy properties. We introduced this method and applied it to a pair of sibling SN Ia (i.e. hosted in the same galaxy) obtained from the ZTF survey to constrain the parameter β to 3.5 ± 0.3. While the historically reported values of β have been much lower, their values have stabilized for the past few years. Our reported values are consistent with the latest literature global values assuming a single β for all SNe, but has a precision that is somewhat worse than the current state of the art. Its advantage is that it is independent of several of the systematic uncertainties of the current methodology. For example, this does not depend on how accurately the population of SN Ia has been modelled in simulations, or how accurately the simulations can represent complex time domain surveys. While we demonstrate this method with a particular pair of siblings, where the constraints on β was expected to be strong (due to the differences

in the best-fitting values of the SN Ia model parameters), the method can be extended to samples of siblings. This would not have been easy in the past, as sibling SN Ia are rare. Thanks to the dramatic improvement in sky survey volume, ongoing surveys are reporting several SN Ia siblings. As we continue to wide-field surveys like ZTF Phase II, YSE, and the LSST on the Vera C. Rubin Observatory, sibling SN Ia will be much more commonly found, allowing this method to be applied to a sample for accurate tests of the SN Ia standardization needed for precision cosmology. If the sample contains siblings whose light-curve shape parameters differ significantly as well, this method can constrain both α and β without other priors. Significant work has gone into developing standardization models (see e.g. Saunders et al. 2018; Hayden, Rubin & Strovink 2019; Léget et al. 2020) that are expected to improve upon SALT2. Such models involve different (and more) free parameters that need to be determined in a manner similar to α and β in the SALT2 model. Presumably, this method can be applied in a similar way, though we have not tried this at all.

A different path to better standardization is improving our understanding of the physical processes underlying the success. One of the most promising routes has been interpreting the physics underlying the colour-dependent term standardization. This could be attributed to intrinsic colour diversity of SN Ia and physics connecting this to the brightness, or/and extinction due to dust in the ISM of the host galaxy, and possibly in the circumstellar environment. Studies for this have used statistical subsamples of SN Ia based on hosts, or samples of individual SN Ia where the extinction parameters are determined through measurements at multiple wavelengths, including space observations in the near-UV (see e.g. Amanullah et al. 2015), or even into the mid-IR (Johansson et al. 2017). Again using the independence of distance/brightness differences of SN Ia in the same galaxy, sibling SN Ia promise an alternative way of probing extinction through accurate measurements of attenuation with well-calibrated systems.

ACKNOWLEDGEMENTS

RB was supported by the research project grant 'Understanding the Dynamic Universe' funded by the Knut and Alice Wallenberg Foundation under Dnr KAW 2018.0067. AG acknowledges support from the Swedish Research Council under Dnr VR 2016-03274 and 2020-03444. SD acknowledges support from the Isaac Newton Trust and the Kavli Foundation through Newton–Kavli fellowship. MR, MS, and Y-LK have received funding from the European Research Council (ERC) under the European Union's Horizon 2020 Framework Programme (grant agreement no. 759194 – USNAC). ECK acknowledges support from the G.R.E.A.T research environment funded by Vetenskapsrådet, the Swedish Research Council, under project number 2016-06012, and support from The Wenner-Gren Foundation.

This study is based on observations obtained with the Samuel Oschin Telescope 48- and the 60-inch Telescope at the Palomar Observatory as part of the Zwicky Transient Facility (ZTF) project. ZTF is supported by the National Science Foundation under Grant No. AST-1440341 and a collaboration including Caltech, IPAC, the Weizmann Institute for Science, the Oskar Klein Center at Stockholm University, the University of Maryland, the University of Washington, Deutsches Elektronen-Synchrotron and Humboldt University, Los Alamos National Laboratories, the TANGO Consortium of Taiwan, the University of Wisconsin at Milwaukee, and Lawrence Berkeley National Laboratories. Operations are conducted by COO, IPAC, and UW. The ZTF forced-photometry service was funded under the Heising-Simons Foundation grant. This work was supported by the GROWTH project funded by the National Science Foundation under Grant No. 1545949.

This study is also based on observations made with the Nordic Optical Telescope, owned in collaboration by the University of Turku and Aarhus University, and operated jointly by Aarhus University, the University of Turku, and the University of Oslo, representing Denmark, Finland, and Norway, the University of Iceland and Stockholm University at the Observatorio del Roque de los Muchachos, La Palma, Spain, of the Instituto de Astrofisica de Canarias. The software used for the analysis and is described below.

Software: NUMPY (van der Walt, Colbert & Varoquaux 2011), ASTROPY (Astropy Collaboration 2013, 2018), SNCOSMO (Barbary et al. 2016), PHOTUTILS (Bradley et al. 2019), ZTFQUERY (Rigault 2018), SWARP (Bertin 2010), HOTPANTS (Becker 2015), ZUDS, FRINGEZ (Medford et al. 2021), LAMBDAR (Wright et al. 2016), PROSPECTOR (Leja et al. 2017), EMCEE (Foreman-Mackey et al. 2013), PYGTC (Bocquet & Carter 2016), MATPLOTLIB (Hunter 2007), and IPAC forced-photometry service.

DATA AVAILABILITY

The ZTF images used for forced photometry are available at the Infrared Science Archive (IRSA) https://irsa.ipac.caltech.edu/Missions/ztf.html and through the ZTF data portal https://www.ztf.caltech.edu/page/dr5#12. The alerts used for initial processing are made available by ZTF in the form of an alert archive https://ztf.uw.edu/, as well as through public brokers that access that ZTF alerts in near real time. The results of running the forced-photometry pipelines that form the main data used in the analysis of this paper are provided in the form of tables in Appendix C.

REFERENCES

Ahn C. P. et al., 2012, ApJS, 203, 21
Alard C., Lupton R. H., 1998, ApJ, 503, 325
Amanullah R. et al., 2010, ApJ, 716, 712
Amanullah R. et al., 2014, ApJ, 788, L21
Amanullah R. et al., 2015, MNRAS, 453, 3300
Astier P. et al., 2006, A&A, 447, 31
Astropy Collaboration, 2013, A&A, 558, A33
Astropy Collaboration, 2018, AJ, 156, 123
Barbary K. et al., 2016, Astrophysics Source Code Library, record ascl:1611.017
Becker A., 2015, Astrophysics Source Code Library, record ascl:1504.004
Bellm E. C. et al., 2019a, PASP, 131, 018002
Bellm E. C. et al., 2019b, PASP, 131, 068003
Bertin E., 2010, Astrophysics Source Code Library, record ascl:1010.068
Betoule M. et al., 2014, A&A, 568, A22
Bocquet S., Carter F. W., 2016, J. Open Source Softw., 1, 46
Bourne N. et al., 2012, MNRAS, 421, 3027
Bradley L. et al., 2019, astropy/photutils: v0.6. Zenodo, available athttps://doi.org/10.5281/zenodo.2533376
Brout D., Scolnic D., 2021, ApJ, 909, 26
Brout D. et al., 2019, ApJ, 874, 150
Bulla M., Goobar A., Dhawan S., 2018, MNRAS, 479, 3663
Burns C. R. et al., 2011, AJ, 141, 19
Burns C. R. et al., 2014, ApJ, 789, 32
Burns C. R. et al., 2020, ApJ, 895, 118
Byler N., Dalcanton J. J., Conroy C., Johnson B. D., 2017, ApJ, 840, 44
Calzetti D., Armus L., Bohlin R. C., Kinney A. L., Koornneef J., Storchi-Bergmann T., 2000, ApJ, 533, 682
Cardelli J. A., Clayton G. C., Mathis J. S., 1989, ApJ, 345, 245
Chabrier G., 2003, PASP, 115, 763
Chambers K. C. et al., 2016, preprint (arXiv:1612.05560)

Childress M. et al., 2013, ApJ, 770, 108
Chotard N. et al., 2011, A&A, 529, L4(C11)
Dettman K. G. et al., 2021, preprint (arXiv:2102.06524)
Dhawan S. et al. 2021, preprint (arXiv:2110.07256)
Foley R. J. et al., 2014, MNRAS, 443, 2887
Foley R. J. et al., 2018, MNRAS, 475, 193
Foreman-Mackey D., Hogg D. W., Lang D., Goodman J., 2013, PASP, 125, 306
Fremling C. et al., 2020, ApJ, 895, 32
Gagliano A., Narayan G., Engel A., Carrasco Kind M., LSST Dark Energy Science Collaboration, 2021, ApJ, 908, 170
Galbany L. et al., 2012, ApJ, 755, 125
Goobar A., 2008, ApJ, 686, L103
Goobar A., Leibundgut B., 2011, Annu. Rev. Nucl. Part. Sci., 61, 251
Goobar A. et al., 2014, ApJ, 784, L12
Graham M. J. et al., 2019, PASP, 131, 078001
Guy J., Astier P., Nobili S., Regnault N., Pain R., 2005, A&A, 443, 781
Guy J. et al., 2007, A&A, 466, 11
Guy J. et al., 2010, A&A, 523, A7(G10)
Hayden B., Rubin D., Strovink M., 2019, ApJ, 871, 219
Hinton S. R. et al., 2019, ApJ, 876, 15
Hoang T., 2017, ApJ, 836, 13
Hoang T., 2021, ApJ, 907, 37
Hunter J. D., 2007, Comput. Sci. Eng., 9, 90
Ivezić Ž. et al., 2019, ApJ, 873, 111
Johansson J. et al., 2017, MNRAS, 466, 3442
Johansson J. et al., 2021, preprint (arXiv:2105.06236)
Jones D. O. et al., 2018a, ApJ, 857, 51
Jones D. O. et al., 2018b, ApJ, 867, 108
Jones D. O. et al., 2021, ApJ, 908, 143
Kasliwal M. M. et al., 2019, PASP, 131, 038003
Kelly P. L., Hicken M., Burke D. L., Mandel K. S., Kirshner R. P., 2010, ApJ, 715, 743
Kelsey L. et al., 2021, MNRAS, 501, 4861
Kessler R., Scolnic D., 2017, ApJ, 836, 56
Kessler R. et al., 2009, ApJS, 185, 32
Kessler R. et al., 2013, ApJ, 764, 48
Kessler R. et al., 2019, MNRAS, 485, 1171
Lampeitl H. et al., 2010, ApJ, 722, 566
Lang D., 2014, AJ, 147, 108
Léget P. F. et al., 2020, A&A, 636, A46
Leja J., Johnson B. D., Conroy C., van Dokkum P. G., Byler N., 2017, ApJ, 837, 170
Licquia T. C., Newman J. A., 2015, ApJ, 806, 96
Liddle A. R., 2007, MNRAS, 377, L74
LSST Science Collaboration, 2009, preprint (arXiv:0912.0201)
Maeda K., Nozawa T., Nagao T., Motohara K., 2015, MNRAS, 452, 3281
Mainzer A. et al., 2014, ApJ, 792, 30
Marriner J. et al., 2011, ApJ, 740, 72
Masci F. J. et al., 2019, PASP, 131, 018003
Medford M. S. et al., 2021, PASP, 133, 064503
Meisner A. M., Lang D., Schlegel D. J., 2017, AJ, 153, 38
Mosher J. et al., 2014, ApJ, 793, 16
Nataf D. M. et al., 2016, MNRAS, 456, 2692
Nobili S., Goobar A., 2008, A&A, 487, 19
Nordin J., Brinnel V., Giomi M., Santen J. V., Gal-Yam A., Yaron O., Schulze S., 2019, Transient Name Server Discovery Report, No. 2019-1202
Nugent P., Kim A., Perlmutter S., 2002, PASP, 114, 803
Perley D. A. et al., 2020, ApJ, 904, 35
Perley D. A., Taggart K., Dahiwale A., Fremling C., 2021, Transient Name Server Classification Report, No. 2021-341
Perlmutter S. et al., 1999, ApJ, 517, 565
Phillips M. M., 1993, ApJ, 413, L105
Piascik A. S., Steele I. A., Bates S. D., Mottram C. J., Smith R. J., Barnsley R. M., Bolton B., 2014, in Ramsay S. K., McLean I. S., Takami H., eds, Proc. SPIE Conf. Ser. Vol. 9147, Ground-based and Airborne Instrumentation for Astronomy V. SPIE, Bellingham, p. 91478H
Planck Collaboration VI, 2020, A&A, 641, A6
Popovic B., Brout D., Kessler R., Scolnic D., Lu L., 2021, ApJ, 913, 49
Riess A. G. et al., 1998, AJ, 116, 1009
Rigault M., 2018, ztfquery, a python tool to access ZTF data. Zenodo, available athttps://doi.org/10.5281/zenodo.1345222
Rigault M. et al., 2015, ApJ, 802, 20
Rigault M. et al., 2020, A&A, 644, A176
Saunders C. et al., 2018, ApJ, 869, 167
Schlafly E. F., Finkbeiner D. P., 2011, ApJ, 737, 103
Schlegel D. J., Finkbeiner D. P., Davis M., 1998, ApJ, 500, 525
Schulze S. et al., 2021, ApJS, 255, 29
Schwarz G., 1978, Ann. Stat., 6, 461
Scolnic D., Kessler R., 2016, ApJ, 822, L35
Scolnic D. M. et al., 2018, ApJ, 859, 101
Scolnic D. et al., 2020, ApJ, 896, L13
Skrutskie M. F. et al., 2006, AJ, 131, 1163
Soraisam M., Matheson T., Lee C.-H., 2021, Res. Notes Am. Astron. Soc., 5, 62
Steele I. A. et al., 2004, in Oschmann J. M., Jr, ed., Proc. SPIE Conf. Ser. Vol. 5489, Ground-based Telescopes. SPIE, Bellingham, p. 679
Sullivan M. et al., 2010, MNRAS, 406, 782
Suzuki N. et al., 2012, ApJ, 746, 85
Thorp S., Mandel K. S., Jones D. O., Ward S. M., Narayan G., 2021, MNRAS, 508, 4310
Tripp R., 1998, A&A, 331, 815
Tripp R., Branch D., 1999, ApJ, 525, 209
van der Walt S., Colbert S. C., Varoquaux G., 2011, Comput. Sci. Eng., 13, 22
Wang L., 2005, ApJ, 635, L33
Wright A. H. et al., 2016, MNRAS, 460, 765
Wright E. L. et al., 2010, AJ, 140, 1868

APPENDIX A: COMPARISON TO SNooPy FITS

For comparison with the SNe Ia SALT2 colour model, we also infer the dust properties of the host galaxy using the SNooPy SN Ia

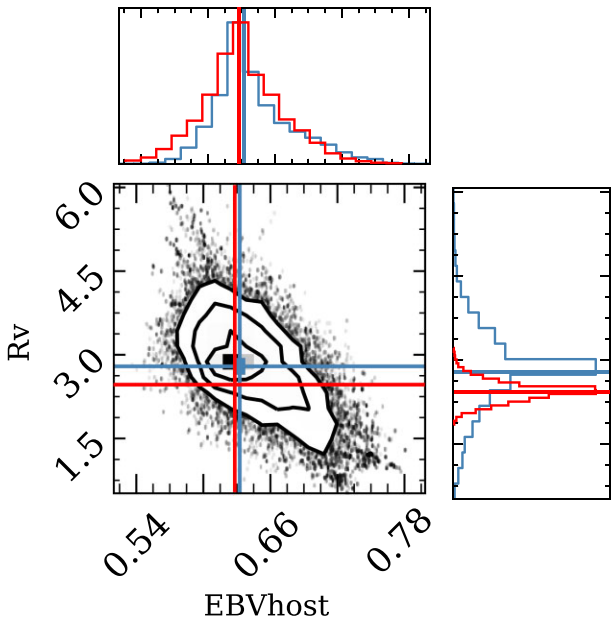

Figure A1. Contour plot showing the inferred R_V and $E(B-V)$ for AT 2019lcj using the SNooPy SN model without any prior (black), with a prior on the unextinguished peak magnitude from SN 2020aewj (red). The best-fitting $R_V = 2.8 \pm 0.7$ and $E(B-V) = 0.63 \pm 0.07$ mag without any prior and $R_V = 2.45 \pm 0.18$ and $E(B-V) = 0.63 \pm 0.07$ with a prior on the peak apparent magnitude from SN 2020aewj.

model. SNooPy is a modular software with different SN Ia models, which can depend on various light-curve shape parameters, to fit template light curves to SN Ia data. While models like the MAX MODEL only fit for the peak magnitude in each filter, we use the COLOUR MODEL, which also fits for the reddening parameters R_V and $E(B-V)$. The colour model templates are a function of the colour stretch, s_{BV}, which is the time since maximum when the $B-V$ colour curve reaches its maximum value, normalized to 30 d. The s_{BV} parameter is shown to be a better ordering parameter than the conventional Δm_{15} light-curve shape, especially for fast-declining SNe Ia (Burns et al. 2014). Fitting the SNooPy colour model to the g, r, i data for AT 2019lcj yields an $R_V = 2.8 \pm 0.71$ and $E(B-V) = 0.63 \pm 0.07$ mag (see Fig. A1). Additionally, similar to the procedure with the SALT2 colour–luminosity and use a prior on the apparent reddening-corrected magnitude of AT 2019lcj from the model fit to SN 2020aewj. This yields an $R_V = 2.45 \pm 0.18$ and $E(B-V) = 0.63 \pm 0.07$ mag. The R_V values from the SNooPy fit are consistent well within 1σ with the $\beta - 1$ from the SALT2 fits.

APPENDIX B: THE DUST MODEL IN BROUT & SCOLNIC (2021)

Brout & Scolnic (2021) propose a change to the prevalent SALT2 methodology positing that the SALT2 colour parameter c obtained from light-curve fits is the sum of two terms:

$$c_{\rm SALT} = c_{\rm int} + E_{\rm dust}, \tag{B1}$$

where $E_{\rm dust}$ is the reddening due to the host galaxy dust and is constrained to be positive, while $c_{\rm int}$ is a colour intrinsic to the SN. Accordingly, they modify the SALT standardization relation

$$\mu = m - M + \alpha\, x_1 - \beta\, c \tag{B2}$$

to

$$\mu = m - M + \alpha\, x_1 - \beta\, c_{\rm int} - R_B\, E_{\rm dust}, \tag{B3}$$

demonstrating that a correlation between R_B and stellar mass of the host galaxy can account for the observed host correlations. A side effect is that the population distribution of $c_{\rm int}$ is a fairly narrow Gaussian with a mean of 0.084 and standard deviation of 0.042. Thus, the well-known red tail in SN populations (see e.g. Scolnic & Kessler 2016) is interpreted as being due to higher values of $E_{\rm dust}$ in this model.

In the context of this work, this model is different from the standard SALT2 model and SALT standardization relation. It has more free parameters, and clearly has a different physical interpretation from the standard SALT2 and SALT standardization relations. In fact, here β that has a universal value is completely independent of R_B, which varies from host galaxy to host galaxy. Brout & Scolnic (2021) demonstrate that a correlation between stellar masses of galaxies and R_B could drive the observed correlations between the standardized

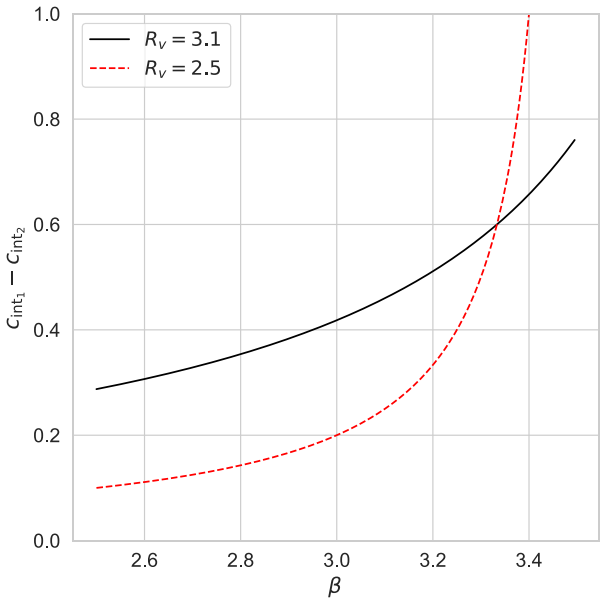

Figure B1. The differences in $c_{\rm int}$ in the model described in Brout & Scolnic (2021) for the pair of siblings described as a function of β (note that this is different from the SALT standardization model β constrained in Section 5 for two choices of R_V).

brightnesses of SN Ia and their host galaxies. We note that the stellar mass of the host galaxy of the siblings is comparable to that of the Milky Way, and thus one might expect this galaxy to have a similar R_V as the Milky Way based on this model.

While we postpone a proper analysis of this model to future work, we can set the SALT2 parameters to the maximum likelihood of the SALT2 parameters as recorded in Table 1. Approximating the individual fits in Table 1, as the difference of SALT2 c parameters is 0.57, the difference in $x1 \sim 0$, and the difference in $m_B^\star$ as $\sim$2, we fix these parameters. Using equations (B1) and (4) to eliminate the terms involving $E_{\rm dust}$, this imposes a relationship between the remaining variables α, β, R_B, and $c_{\rm int}$. Utilizing the Pantheon priors on α, this gives us the difference in $c_{\rm int}$, $\Delta c_{\rm int} = c^1_{\rm int} - c^2_{\rm int}$ for different values of R_B and β. In Fig. B1, we show the values of $\Delta c_{\rm int}$ for different choices β where we have fixed R_V to 3.1 or 2.5. Since we know the population distribution of $c_{\rm int}$ is a normal distribution of known mean and variance, we can see that the PDF of the $\Delta c_{\rm int}$ is a normal distribution with mean approximately 1.6 and a standard deviation of 0.06.

APPENDIX C: PHOTOMETRY TABLES USED

Note that these tables (Tables C1 and C2) are also made available in electronic format.

Table C1. Light-curve points for AT 2019lcj used in the analysis. The zero points (ZP) are in the AB system.

JD (d)	Band	Flux (counts)	Flux_err (counts)	ZP	Seeing (arcsec)	$m_{\rm lim}$ (mag)
245 8655.79	p48g	18.72	37.23	25.93	2.9745	19.91
245 8662.94	p48g	56.02	22.66	26.06	1.9512	20.79
245 8663.97	p48g	65.35	35.57	25.58	2.1306	19.75
245 8663.97	p48g	− 58.13	36.12	25.54	2.174	19.64
245 8672.81	p48g	143.99	18.31	26.02	2.4073	20.73
245 8672.83	p48g	93.51	18.66	26.04	1.9574	20.96
245 8673.80	p48g	181.56	23.37	26.09	2.2867	20.62
245 8673.83	p48g	167.44	19.76	26.08	1.9766	20.94
245 8674.83	p48g	216.91	28.24	26.11	1.779	20.64
245 8674.85	p48g	266.67	22.44	26.08	2.0647	20.74
245 8675.81	p48g	183.23	36.75	26.07	1.9471	20.28
245 8675.85	p48g	243.35	31.69	26.06	1.8856	20.45
245 8678.78	p48g	369.44	52.74	26.06	2.6459	19.58
245 8679.79	p48g	354.50	58.68	26.09	2.1964	19.67
245 8680.70	p48g	497.51	65.23	26.08	2.1413	19.58
245 8681.70	p48g	353.79	66.10	26.07	2.3575	19.46
245 8682.70	p48g	416.38	51.36	26.09	2.0582	19.86
245 8683.78	p48g	404.32	49.62	26.09	1.9435	19.96
245 8684.77	p48g	412.83	41.90	25.99	2.5365	19.86
245 8685.87	p48g	430.13	43.94	26.02	2.2696	19.90
245 8693.77	p48g	353.75	22.05	26.05	2.2308	20.69
245 8696.76	p48g	275.83	22.50	26.08	1.998	20.75
245 8696.81	p48g	278.77	22.62	26.06	1.9962	20.75
245 8697.83	p48g	250.44	23.89	26.04	1.865	20.72
245 8699.81	p48g	165.57	24.34	26.01	2.0476	20.63
245 8700.76	p48g	236.76	23.21	26.07	2.0132	20.70
245 8700.81	p48g	252.79	23.53	26.05	1.8405	20.75
245 8701.81	p48g	112.43	23.90	25.96	1.9193	20.62
245 8702.81	p48g	145.08	24.18	25.97	1.8191	20.65
245 8703.69	p48g	106.19	34.28	25.93	2.6593	19.99
245 8703.81	p48g	201.14	24.65	25.99	1.9368	20.61
245 8704.81	p48g	136.22	34.00	26.01	2.3005	20.13
245 8704.88	p48g	122.88	26.77	25.89	2.7116	20.19
245 8704.90	p48g	134.62	27.42	25.87	2.7151	20.12
245 8705.73	p48g	127.43	41.91	26.03	1.7947	20.16
245 8705.91	p48g	163.97	27.59	25.88	2.4236	20.22
245 8706.68	p48g	123.65	45.22	26.11	1.951	20.07
245 8706.73	p48g	46.97	46.01	26.03	1.928	20.04
245 8707.91	p48g	125.95	48.56	25.97	2.0606	19.81
245 8708.66	p48g	97.68	55.14	26.07	1.6609	19.93
245 8708.73	p48g	189.82	55.55	26.05	2.2432	19.69
245 8708.89	p48g	− 9.06	62.65	25.97	2.0441	19.52
245 8709.73	p48g	151.77	61.24	26.10	1.9602	19.70
245 8710.66	p48g	206.42	63.87	26.10	1.6057	19.83
245 8710.71	p48g	97.73	68.72	26.10	2.0118	19.56
245 8710.73	p48g	92.19	69.68	26.05	1.9891	19.54
245 8711.71	p48g	72.08	62.48	26.08	1.7558	19.78
245 8711.76	p48g	77.31	65.87	26.07	1.8454	19.67
245 8714.71	p48g	67.30	37.72	26.04	1.8598	20.27
245 8715.80	p48g	15.07	42.89	26.02	1.8539	20.10
245 8716.82	p48g	47.07	40.81	26.00	1.9475	20.10
245 8717.80	p48g	106.93	34.90	25.98	2.1284	20.18
245 8718.82	p48g	80.48	31.08	25.91	2.5508	20.10
245 8719.80	p48g	85.00	26.32	25.90	2.511	20.25
245 8720.82	p48g	45.66	27.68	25.90	1.8968	20.43
245 8722.80	p48g	67.01	26.90	25.96	1.7849	20.55
245 8725.68	p48g	59.00	24.40	25.94	2.5194	20.40
245 8725.70	p48g	117.88	24.53	26.02	2.1454	20.57
245 8725.80	p48g	66.25	26.46	26.01	1.895	20.58
245 8726.80	p48g	8.70	27.05	25.94	2.2034	20.38
245 8727.77	p48g	40.43	26.43	25.97	1.8142	20.57
245 8727.82	p48g	12.92	28.40	25.93	1.9406	20.41
245 8728.68	p48g	57.67	25.33	25.96	1.6413	20.65
245 8730.80	p48g	16.70	28.23	25.85	2.0934	20.28

Table C1 – *continued*

JD (d)	Band	Flux (counts)	Flux_err (counts)	ZP	Seeing (arcsec)	$m_{\rm lim}$ (mag)
245 8732.65	p48g	48.68	34.33	25.98	1.8434	20.29
245 8732.68	p48g	19.28	34.25	25.98	1.6656	20.36
245 8732.69	p48g	8.11	33.99	25.97	1.8042	20.32
245 8732.79	p48g	29.79	26.97	25.95	1.7882	20.54
245 8733.66	p48g	11.55	36.81	26.03	1.9404	20.25
245 8733.79	p48g	96.79	33.92	25.89	2.5993	19.92
245 8733.81	p48g	61.58	31.29	25.91	2.3659	20.11
245 8733.83	p48g	45.68	29.15	25.84	2.6269	20.05
245 8734.69	p48g	91.92	39.74	25.96	2.7377	19.85
245 8734.72	p48g	13.64	40.51	25.92	2.9513	19.74
245 8734.80	p48g	33.17	40.78	25.95	2.3262	19.85
245 8735.79	p48g	59.31	47.94	25.93	2.1473	19.74
245 8736.80	p48g	3.06	55.10	25.85	2.8398	19.33
245 8659.68	p48i	− 98.84	37.22	25.52	1.3288	19.98
245 8663.68	p48i	− 39.71	28.13	25.45	1.8868	19.90
245 8672.94	p48i	131.23	30.23	25.48	1.8611	19.90
245 8679.76	p48i	438.90	36.02	25.56	1.5662	19.96
245 8685.80	p48i	293.17	35.28	25.52	1.461	19.98
245 8690.83	p48i	391.43	31.57	25.48	1.4088	20.12
245 8696.68	p48i	230.51	31.10	25.52	1.4778	20.15
245 8701.91	p48i	180.12	35.62	25.41	1.4528	19.91
245 8710.75	p48i	166.77	44.15	25.54	1.5235	19.73
245 8715.81	p48i	237.98	35.97	25.51	1.6284	19.90
245 8719.66	p48i	216.90	33.67	25.46	1.6936	19.86
245 8732.83	p48i	144.40	33.99	25.42	1.6258	19.83
245 8654.86	p48r	76.85	44.48	26.02	2.2151	19.92
245 8657.87	p48r	− 43.84	33.28	26.04	1.9803	20.39
245 8661.83	p48r	− 98.84	25.44	26.05	1.9287	20.69
245 8661.83	p48r	9.59	24.91	26.05	2.0323	20.70
245 8662.75	p48r	13.14	28.98	26.08	1.7381	20.59
245 8663.83	p48r	− 80.74	28.56	26.05	2.013	20.54
245 8663.84	p48r	− 6.23	28.78	26.06	1.966	20.56
245 8663.84	p48r	30.49	29.50	26.09	1.6037	20.67
245 8665.85	p48r	24.15	28.52	26.11	1.5575	20.70
245 8672.72	p48r	207.37	29.31	26.05	1.9369	20.51
245 8673.72	p48r	358.72	31.29	26.13	1.4066	20.64
245 8677.77	p48r	550.80	45.17	26.09	1.5020	20.26
245 8678.72	p48r	681.85	47.77	26.12	1.4399	20.24
245 8679.74	p48r	773.15	50.47	26.12	1.5577	20.15
245 8680.76	p48r	734.08	54.11	26.08	2.1612	19.77
245 8681.76	p48r	753.90	55.16	26.06	2.2524	19.73
245 8682.76	p48r	683.84	49.04	26.12	1.489	20.18
245 8683.75	p48r	782.34	44.65	26.10	1.5661	20.27
245 8684.74	p48r	697.07	37.29	26.02	2.2422	20.15
245 8685.84	p48r	830.17	40.62	26.09	1.5865	20.32
245 8688.89	p48r	864.20	38.46	26.03	1.523	20.34
245 8690.85	p48r	677.57	32.01	26.02	1.3362	20.56
245 8691.68	p48r	723.03	29.70	26.05	1.53	20.62
245 8692.83	p48r	594.66	32.16	26.04	1.6437	20.50
245 8693.72	p48r	574.09	31.92	26.03	1.5733	20.55
245 8694.70	p48r	579.28	30.94	26.10	1.395	20.68
245 8695.78	p48r	355.74	38.66	25.21	1.9794	19.30
245 8696.78	p48r	609.70	28.70	26.09	1.5222	20.70
245 8696.86	p48r	468.21	29.53	26.06	1.6503	20.60
245 8697.80	p48r	529.99	29.90	26.06	1.7317	20.59
245 8699.78	p48r	456.27	31.49	26.05	1.5015	20.56
245 8701.78	p48r	345.30	35.18	25.78	1.7682	20.08
245 8702.78	p48r	313.64	33.10	25.96	1.3461	20.48
245 8703.68	p48r	344.44	36.48	26.00	1.9797	20.24
245 8703.78	p48r	464.35	34.31	26.03	1.7509	20.39
245 8704.78	p48r	322.64	37.13	26.03	2.2181	20.11
245 8705.68	p48r	416.77	41.75	26.06	1.7215	20.24
245 8705.70	p48r	595.86	42.53	26.07	1.4837	20.30
245 8706.70	p48r	510.31	43.66	26.10	1.4447	20.29

Table C1 – *continued*

JD (d)	Band	Flux (counts)	Flux_err (counts)	ZP	Seeing (arcsec)	$m_{\rm lim}$ (mag)
245 8706.84	p48r	415.71	46.48	26.05	1.5837	20.16
245 8707.70	p48r	371.49	46.63	26.09	1.4241	20.26
245 8709.70	p48r	426.38	53.09	26.09	1.7109	20.03
245 8710.69	p48r	354.46	57.26	26.10	1.4671	20.01
245 8711.69	p48r	334.41	52.62	26.11	1.5541	20.07
245 8714.69	p48r	441.02	33.92	26.07	1.5714	20.55
245 8715.77	p48r	219.52	40.72	26.08	1.486	20.34
245 8716.79	p48r	275.66	40.50	26.06	1.654	20.28
245 8717.77	p48r	335.43	35.88	26.05	1.6434	20.41
245 8718.79	p48r	185.96	33.32	25.99	2.1706	20.25
245 8719.77	p48r	115.37	33.86	25.91	2.6513	20.00
245 8720.79	p48r	262.36	34.92	25.99	1.5167	20.42
245 8722.77	p48r	340.10	33.25	26.03	1.4654	20.50
245 8723.80	p48r	95.53	32.70	26.01	1.6926	20.50
245 8725.77	p48r	245.73	32.49	26.06	1.3984	20.56
245 8726.77	p48r	235.97	34.85	26.04	1.5069	20.49
245 8727.80	p48r	186.60	35.37	26.02	1.4836	20.42
245 8730.64	p48r	107.54	38.77	25.96	1.6622	20.23
245 8730.77	p48r	152.84	37.58	25.93	1.8356	20.15
245 8732.77	p48r	107.84	36.56	26.04	1.3995	20.44
245 8733.74	p48r	199.48	39.83	26.07	1.7258	20.28
245 8733.77	p48r	11.14	41.14	26.04	1.7149	20.23
245 8734.77	p48r	116.41	43.88	26.02	1.8755	20.06
245 8734.82	p48r	130.66	44.73	25.94	2.3806	19.78
245 8736.78	p48r	108.34	52.57	25.99	1.9647	19.84
245 8737.79	p48r	94.51	57.59	25.98	2.1669	19.64

Table C2. Light-curve points for SN 2020aewj used in the analysis. The zero points (ZP) are in the AB system.

JD (d)	Band	Flux (counts)	Flux_err (counts)	ZP	Seeing (arcsec)	$m_{\rm lim}$ (mag)
245 8877.02	p48g	742.07	27.51	26.08	2.6403	20.24
245 8880.98	p48g	1473.84	28.76	25.99	2.7017	20.21
245 8882.02	p48g	2005.69	27.94	26.12	2.2046	20.49
245 8891.97	p48g	2594.26	60.44	26.08	2.5028	19.51
245 8893.99	p48g	2401.47	46.10	26.09	2.1244	19.95
245 8899.05	p48g	2023.54	26.14	26.18	1.9566	20.74
245 8900.04	p48g	1777.22	27.06	26.10	2.427	20.38
245 8901.04	p48g	773.74	33.82	25.33	2.0688	19.53
245 8904.03	p48g	1337.40	24.73	26.15	2.0789	20.73
245 8909.05	p48g	852.24	44.56	26.16	2.3004	19.96
245 8912.05	p48g	600.80	33.44	26.03	2.8533	20.06
245 8914.02	p48g	456.64	26.50	25.93	2.0779	20.46
245 8914.94	p48g	400.14	58.13	25.97	2.0866	19.56
245 8915.97	p48g	443.95	66.20	26.03	2.2789	19.43
245 8942.00	p48g	187.59	20.76	26.00	2.8643	20.53
245 8874.03	p48r	320.95	34.97	26.14	1.8541	20.46
245 8876.05	p48r	457.65	30.19	26.04	2.5855	20.24
245 8877.06	p48r	735.35	34.38	26.18	1.7229	20.54
245 8878.02	p48r	887.10	32.10	26.10	2.205	20.34
245 8879.07	p48r	947.57	45.33	25.98	2.8889	19.71
245 8881.04	p48r	1502.91	34.15	26.11	2.2954	20.29
245 8882.05	p48r	1827.11	34.74	26.15	1.8957	20.46
245 8886.05	p48r	2295.86	36.98	26.14	2.0698	20.35
245 8887.06	p48r	2408.75	49.58	26.19	1.6498	20.22
245 8888.05	p48r	2480.49	63.14	26.18	1.7269	19.90
245 8894.05	p48r	2516.26	45.71	26.17	1.5729	20.34
245 8895.04	p48r	2546.97	42.90	26.18	1.6562	20.37
245 8895.99	p48r	2402.58	39.21	26.16	1.8695	20.35
245 8899.03	p48r	2148.01	32.88	26.17	1.5319	20.67
245 8899.98	p48r	1840.99	36.65	26.10	2.4675	20.10

Table C2 – *continued*

JD (d)	Band	Flux (counts)	Flux_err (counts)	ZP	Seeing (arcsec)	$m_{\rm lim}$ (mag)
245 8904.01	p48r	1585.96	32.71	26.16	1.8345	20.59
245 8908.99	p48r	1382.19	34.75	26.14	1.9151	20.46
245 8912.99	p48r	1361.77	38.80	26.09	1.7249	20.39
245 8914.00	p48r	975.57	39.22	25.84	1.5394	20.18
245 8937.02	p48r	598.16	36.08	26.13	1.784	20.48
245 8941.01	p48r	288.69	38.65	25.73	1.8366	19.96

This paper has been typeset from a TEX/LATEX file prepared by the author.